Measurement 193 (2022) 110910

Contents lists available at ScienceDirect

Measurement

journal homepage: www.elsevier.com/locate/measurement

A numerical and experimental analysis of multi-hole orifice in turbulent flow

Anna Golijanek-Jędrzejczyk [a,*], Andrzej Mrowiec [b], Sławosz Kleszcz [c], Robert Hanus [d], Marcin Zych [e], Marek Jaszczur [c]

[a] Gdańsk University of Technology, Faculty of Electrical and Control Engineering, Gdańsk, Poland
[b] Calisia University, Polytechnic Faculty, Kalisz, Poland
[c] AGH University of Science and Technology, Faculty of Energy and Fuels, Kraków, Poland
[d] Rzeszów University of Technology, Faculty of Electrical and Computer Engineering, Rzeszów, Poland
[e] AGH University of Science and Technology, Faculty of Geology, Geophysics and Environmental Protection, Kraków, Poland

ARTICLE INFO

Keywords:
Multi-hole orifice
Numerical analysis
CFD
Turbulent flow
Flow rate measurement

ABSTRACT

In this research study, the comprehensive metrological analysis is investigated for a 4-hole orifice with module $m = 0.25$ installed in the pipeline with an internal diameter of 50 mm. A detailed numerical simulation was performed for the turbulence models: *k-ε-realizable* and *k-ω-BSL*. The novelties of the research include model validation by comparing the results of numerical studies with the experiment conducted in the area of developing turbulent flow in the range of Reynolds numbers from 4,200 to 19,000. Such validated models are sought by the system designers and can be used for further analyses and optimisation of this orifice in this flow type. The multi-hole orifices are less sensitive to flow disturbances than the standardized standard centric orifice. In addition, orifices of this type can be mounted in installations with much shorter sections upstream and downstream of the orifice - which is very often the case in industrial flow installations.

1. Introduction

Flow rate measurements are used in many fields, such as power engineering, fuel industry, environmental engineering, biology, medicine, etc. [1]. Orifice measurements are one of the oldest, simplest and, at the same time, most common methods of measuring the flow rate [2–4]. This does not mean that they do not require further in-depth metrological analyses in terms of accuracy and selection of the damming pressure reception point. One of the best-known orifice designs is the centric orifice, however, a very promising alternative is a multi-hole orifice, which, unlike the centric orifice, has more than one hole. The holes made in the orifice can have a circular or slotted shape [5], and their number can be even or odd. They can be arranged at different angles to the symmetry axis of the orifice as well as to the measuring points used to record the backpressure.

The literature presents experimental and numerical studies that analyse different numbers of holes and their arrangements in multi-hole orifice design solutions and mainly focus on the effect of different numbers of holes and their distribution, taking into account the value of the flow coefficient and compactness of holes, on the resulting permanent pressure loss.

In [6] the authors investigated 15 different variations of these parameters for a pipeline with a diameter of 114.3 mm. It was found that the dominant geometrical factor influencing the pressure loss coefficient is the flow coefficient, while the number of holes and their arrangement turned out to have less influence on the pressure loss characteristics. The dependence of the number of holes on the flow coefficient was also observed, with a strong impact on the pressure loss coefficient. The authors show that the influence of the number of holes is dominant at lower values of the flow coefficient and decreases at its higher values.

The review of publications [7–9] made it possible to conclude that multi-hole orifices are characterized by a lower pressure loss and lower turbulence intensity in the flowing stream than single hole orifices. In those works, it was observed that the water stream flows through the multi-hole orifice with different values of the equivalent throat coefficient. This advantage is observed due to the more stable distribution of the velocity field downstream of the multi-hole orifice as a result of the larger number of flow openings. In this case, a slight decrease in the measuring backpressure at the orifice itself is observed, while the value

* Corresponding author.
E-mail addresses: anna.golijanek-jedrzejczyk@pg.edu.pl (A. Golijanek-Jędrzejczyk), a.mrowiec@akademiakaliska.edu.pl (A. Mrowiec), slawosz.kleszcz@frapol.com.pl (S. Kleszcz), rohan@prz.edu.pl (R. Hanus), zych@agh.edu.pl (M. Zych), jaszczur@agh.edu.pl (M. Jaszczur).

https://doi.org/10.1016/j.measurement.2022.110910
Received 27 October 2021; Received in revised form 8 February 2022; Accepted 15 February 2022
Available online 17 February 2022

Nomenclature:

a	slope [-]
b	intercept [-]
d_n	diameter of one of the holes (identical) in the orifice [m]
C	discharge coefficient [-]
D	pipe internal diameter [m]
q_V	volume flow [dm^3/s]
k	kinetic energy of turbulence [m^2/s^2]
m	orifice module [-]
n	number of holes in a multi-hole orifice [-]
p	static pressure [Pa]
P_k	generation of turbulence kinetic energy due to the mean velocity gradients [J]
P_b	generation of turbulence kinetic energy due to buoyancy [J]
R^2	determination coefficient [-]
Re	Reynolds number [-]
S	strain tensor [-]
t	time [s]
T	fluid temperature [°C]
u_i	velocity component [m/s]
v	average flow velocity [m/s]
x	distance [m]
β	orifice diameter ratio [-]
δ	relative pressure difference [%]
ε	dissipation [m^2/s^3]
ε_v	expansion coefficient [-]
Δp	difference pressure [Pa]
Δt	sampling time [s]
ν	kinematic viscosity [m^2/s]
μ_t	turbulent viscosity [m^2/s]
ρ	fluid density [kg/m^3]
ω	turbulent dissipation rate [1/s]

of the discharge coefficient C increases, compared to the commonly used single hole orifice.

Currently, due to the increasing availability and simplicity of checking the properties of flowmeters using numerical simulations [10,11], more and more researchers are searching for orifices that would be characterized by a constant value of the flow coefficient over a wide range of Reynolds numbers [12]. In [13,14], the metrological properties of multi-hole orifices have been analysed based on experimental measurements and numerical simulations in a fully developed turbulent flow. Bagade et al. [13] determined the discharge coefficient C for the 4, 9, and 13-hole orifices with water flow, while the other study compared the coefficient C for the 6-hole orifice with the coefficient for the centric orifices for moist air flow [14].

Typically, the literature results obtained from numerical simulations for multi-hole orifices are shown using various numerical models. However, the results of neither the experimental measurements nor the analytical solutions were used to verify these numerical models. The investigation carried out using the k-ε turbulence model for an orifice with diameter ratio $\beta = 0.6$ and the number of holes from 4 to 25 has been presented by Mehendra et al. [15]. The results were shown in the form of the velocity field and pressure distribution around the orifice for each analysed case. Similar studies, with the same turbulence model k-ε used to simulate flow through a multi-hole orifice with substitute orifice diameter ratios β equal to 0.5; 0.55; 0.6 and 0.7, were carried out in the pipeline with an internal diameter of $D = 70.3$ mm [16]. Another pipeline, with an internal diameter of DN80 and a substitute orifice diameter ratio $\beta = 0.45$, has been analysed by Hao et al. [17]. In that case, the flow field was determined by optimizing the shape of the flow holes in the orifice to increase the accuracy of the measurements.

In works [18,19], the authors calculated pressure drops and flow coefficients for different geometric parameters (number of holes and their arrangement) and flow parameters of the investigated orifices using numerical simulations. They also presented the discussion of the advantages of the proposed solutions.

Mrowiec [20] estimated the uncertainty of the flow measurement for a four-hole orifice. An attempt was made to estimate the uncertainty of determining the discharge coefficient C with the equivalent orifice diameter ratio $\beta = 0.5$ for not fully developed turbulent flow ($Re <$ 20,000). The estimated value of uncertainty was shown to not differ from that for the centric orifice with the same reduction.

Multi-hole orifices increase the anti-disturbance capability compared to the standard orifice with a single hole. Studies carried out have shown that the reduction of the required length of the developed pipeline sections upstream and downstream of the multi-hole orifice is significant. This conclusion is crucial for industrial and technological systems, where often the required length of the measuring sections for a standard single hole orifice cannot be ensured. This advantage of an orifice can be used when designing an industrial ball shut-off valve with a function that enables fluid flow measurement, as shown by Romanik & Rogula [21]. In that case, short measuring sections resulting from the dimensions of the ball valve made it possible to integrate the measuring multi-hole orifice into the valve ball.

The literature analysis shows that the multi-hole orifices are also extremely promising due to their high flow rate stability. However, they still require extensive optimization and analysis in terms of the number of holes and their location. These analyses can be performed based on computer modelling, provided that the applied model has been properly verified experimentally.

In the literature the large number of numerical analyses can be found. However, presented models were never detailed validated and for this reason, it is not obvious whether they can be used for accurate orifices analysis. The aim of this research study is the evaluation the numerical model used to analyse a multi-hole orifice with module $m =$ 0.25.

The novelties of the research include model validation by comparing the results of numerical studies with the experiment conducted in the area of developing turbulent flow, i.e., in the range of Reynolds numbers from 4200–19,000. In the available literature, no such studies can be found on multi-hole orifices, which would provide detailed validation of numerical models used in this range of Reynolds numbers. Such validated models are very much sought after by the system designers and can be used for further analyses and optimisation of this orifice in this flow type.

The numerical calculations, as well as experimental measurements carried out so far and presented in the literature clearly, indicate that the multi-hole orifices are less sensitive to flow disturbances than the standardized standard centric orifice. In addition, orifices of this type can be mounted in installations with much shorter sections upstream and downstream of the orifice - which is very often the case in industrial flow installations. In the literature, most publications concerning multi-hole orifices mainly present the results of simulation and numerical tests, occasionally supported by experimental (flow) tests. There are no studies in the literature presenting the results of numerical calculations (simulations in Ansys Fluent software) supported by experimental tests for a four-hole orifice with a module of 0.25 for turbulent flow with low values of Reynolds numbers ($Re <$ 20000).

2. The geometry of analysed multi-hole orifice

Fig. 1 shows a diagram of the 4-hole orifice analysed in this research

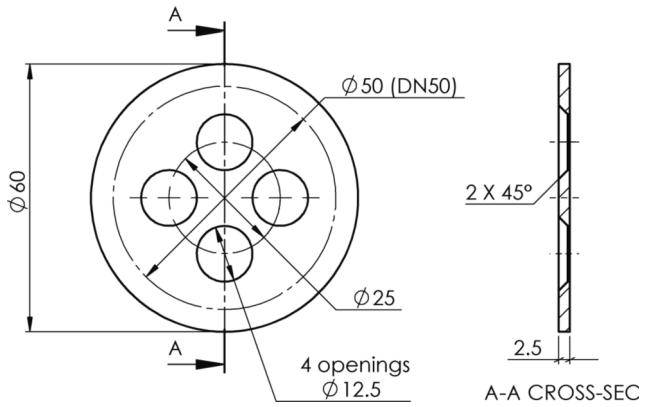

Fig. 1. Sketch of the analysed orifice.

work.

The orifice is made of brass. It has the diameter DN50 and the diameter ratio

$\beta = 0.5$ (module $m = 0.25$). Modulus, i.e. the ratio of the narrowing hole area to the pipeline cross-sectional area.

To determine the theoretical volume flux of an incompressible fluid flowing through a measuring orifice, we use the Bernoulli equation in conjunction with the continuity equation. The flow of volume determined in this way refers to the flow of perfect, non-sticky fluids. In the case of the flow of real fluids (e.g. water), the viscosity present in them causes additional flow losses related to the conversion of kinetic energy into heat. Taking this effect into account, a flow coefficient was introduced into the theoretical equation for calculating the volume flow, which takes into account its reduction [2]. Thus, we obtain the dependence on the actual fluid volume flow. The fluid volume flow q_v flowing through the tested multi-hole orifice (with four identical holes made according to Fig. 1) can be written by the relationship:

$$q_v = \frac{C \cdot \varepsilon_v \cdot n \cdot \pi \cdot d_n^2}{4 \cdot \sqrt{1 - m^2}} \cdot \sqrt{\frac{2 \cdot \Delta p}{\rho}} \tag{1}$$

where: C - discharge coefficient [-],
ε_v - expansion coefficient (for liquids $\varepsilon_v = 1$) [-],
n - number of holes in a multi-hole orifice ($n = 4$) [-],
d_n - the diameter of one of the holes (identical) in the orifice [m],
D - pipe diameter [m],
m - orifice module ($m = n \cdot d_n^2 / D^2$) [-],
Δp - difference pressure before and after the orifice [Pa],
ρ - fluid density [kg/m^3].

Analysing the issue of turbulence in the zone directly in front of and behind the multi-hole (4-hole) orifice, it can be concluded that:

- during the flow, liquid particles on the front surface in front of the orifice are accumulated, resulting in a local, slight increase in pressure,
- the flowing liquid, after flowing through the holes in the multi-hole orifice, hits the zones of reduced pressure and properties that tend to vacuum, causing chaotic swirls.

This phenomenon results from the inertia of the liquid molecules, which are not able to quickly fill these areas (zones) with reduced pressure. As a result of the sudden pressure change behind the orifice, interwoven vortices are formed behind each of the flow openings. Therefore, for a multi-hole orifice, the velocity profile becomes stable at a distance of two pipe diameters downstream of it; compared to a standard orifice, this distance is at least about four times smaller. In industrial flow systems, there are practically no rectilinear sections of the pipeline of the length required by the standards. Therefore, this type of orifice is a sought-after solution that is perfect for short, straight sections with a length of approximately two pipeline diameters upstream and downstream of the orifice.

The experimental measurement was carried out in an individually designed casing, which allowed back pressure measurements: point (P_1, P_2), flange (K_1, K_2) and D-$D/2$, in a hydraulic flow pipeline with internal diameter 50 mm (DN50).

The experimental measurements were carried out for the pairs of the stagnation pressure sampling points specified in the ISO 5167–2 standard, as the measurement of:

- parathyroid point (marked in the figure as P_1, P_2),
- flange point (marked in the figure as K_1, K_2),
- point - along with the length D in front of the orifice and $D/2$ behind the orifice (marked in the drawing as D-$D/2$).

Standardized points for back pressure reception are shown in Fig. 2.

3. CFD modelling

The flowmeter based on the designed 4-hole orifice was subjected to numerical analyses. Simulations were conducted using the Ansys Fluent solver. In the current studies, a three-dimensional (3D) model of the orifice has been developed to analyse the fluid flow and pressure drop. The mesh was generated in the entire domain, including the upstream and downstream sections of the pipeline. In order to take into account the processes at the wall, the inflation layer along the pipelane was generated. After some of the preliminary tests, a final mesh consisting of 2,000,000 elements was used to guarantee mesh-independent results. Fig. 3 shows the computational domain with the orifices mounted inside the pipeline and the pressure measurement points.

When generating the mesh for the orifice domain and the surrounding domain, attention was paid to the holes and their chamfering. The final version of the mesh, verified based on a series of preliminary tests, is shown in Fig. 4 (a)-(b).

To model the turbulent flow, two preselected turbulent models were used. The first was the *k-ε-realizable* model, being the modification of the standard *k-ε* model, while the second was the *k-ω-BSL* model. The model constants for both equations used standard value, and they were not changed. We analysed several different models (before preselection for proposed models) but according to our knowledge (also from literature) and experience as well as test analysis, the proposed two models are very promising robust and accurate for this type of calculations.

The first is *k-ε* model [22,23] known as a semi-empirical 2-equation (2–3), eddy viscosity model, which is based on the Boussinesq hypothesis. In this model, the Reynolds stresses are expressed in terms of mean velocity gradients, and the turbulent eddy viscosity is related to the turbulent kinetic energy and the dissipation rate of the turbulent kinetic energy.

The *k–ε* turbulence models incorporate, on average, the influence of

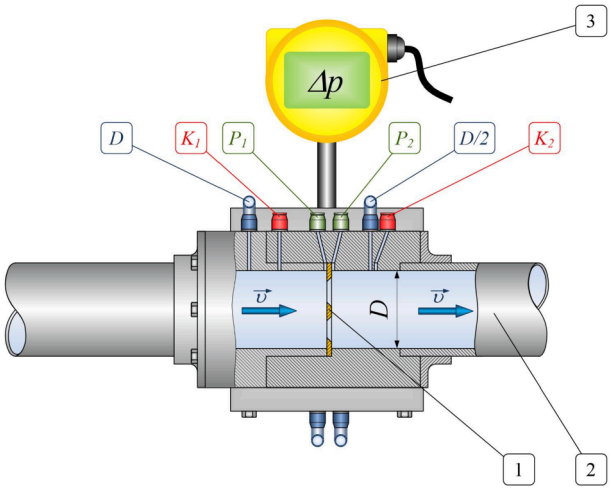

Fig. 2. Location of backpressure points: 1- orifice plate, 2- measuring section of the pipeline, 3- differential pressure converter.

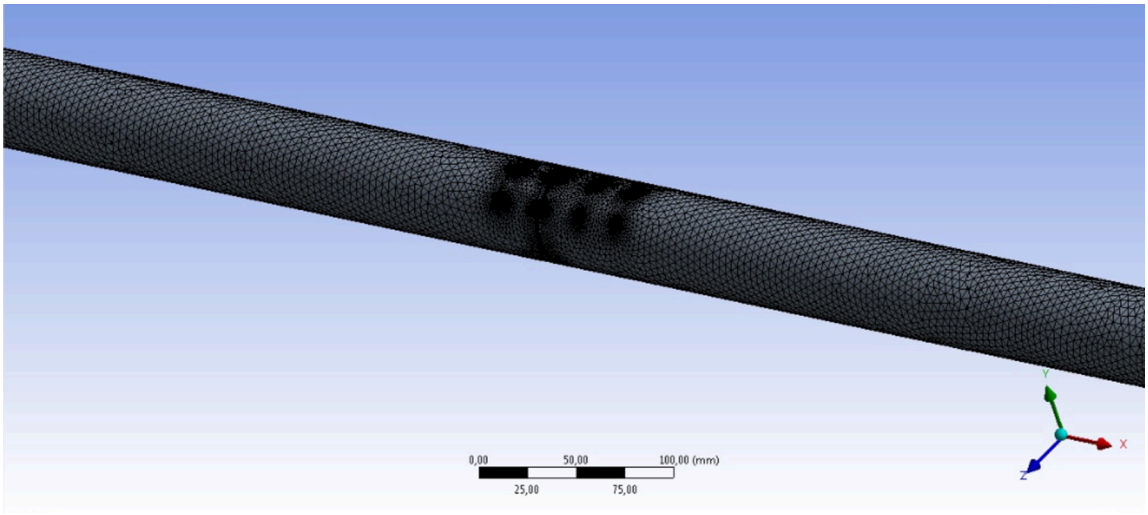

Fig. 3. Computational domain.

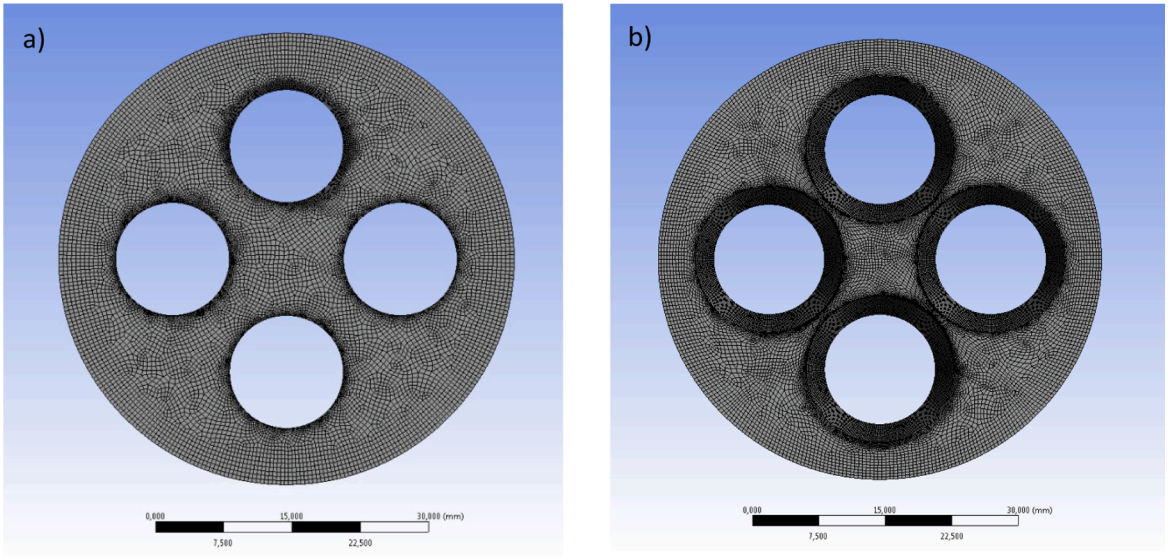

Fig. 4. Numerical grid of the multi-hole orifice: a) top view – inflow and b) back view – outflow.

turbulent eddies (Reynolds stresses) through turbulent viscosity, which is related to the fluid rate of strain. The realizable *k-ε* model is used because this model contains an improved formulation for turbulent viscosity (4), which provides much better results than other turbulence models for this type of geometry.

For turbulent kinetic energy *k* [22]:

$$\frac{\partial(\rho k)}{\partial t}+\frac{\partial(\rho k u_i)}{\partial x_i}=\frac{\partial}{\partial x_j}\left[\left(\mu+\frac{\mu_t}{\sigma_k}\right)\frac{\partial k}{\partial x_j}\right]+P_k+P_b-\rho\varepsilon \tag{2}$$

where ρ is denesity, t is time, u_i is velocity component, μ_t is turbulent viscosity, P_k is the generation of turbulence kinetic energy due to the mean velocity gradients, P_b is the generation of turbulence kinetic energy due to buoyancy, ε is dissipation and σ_k is the constant.

For dissipation ε [22]:

$$\frac{\partial(\rho\varepsilon)}{\partial t}+\frac{\partial(\rho\varepsilon u_i)}{\partial x_i}=\frac{\partial}{\partial x_j}\left[\left(\mu+\frac{\mu_t}{\sigma_\varepsilon}\right)\frac{\partial\varepsilon}{\partial x_j}\right]+C_{1\varepsilon}\frac{\varepsilon}{k}(P_k+C_{3\varepsilon}P_b)-C_{2\varepsilon}\rho\frac{\varepsilon^2}{k} \tag{3}$$

where $\sigma_\varepsilon, C_{1\varepsilon}, C_{3\varepsilon}, C_{2\varepsilon}$ are the constant.

The *k-ε-realizable* model differ from *k-ε* in case of calculation the turbulent dissipation rate. In this case equation (3) became:

$$\frac{\partial(\rho\varepsilon)}{\partial t}+\frac{\partial(\rho\varepsilon u_i)}{\partial x_i}=\frac{\partial}{\partial x_j}\left[\left(\mu+\frac{\mu_t}{\sigma_\varepsilon}\right)\frac{\partial\varepsilon}{\partial x_j}\right]+\rho C_1 S\varepsilon-\rho C_2\frac{\varepsilon^2}{k+\sqrt{\vartheta\varepsilon}}+C_{1\varepsilon}\frac{\varepsilon}{k}C_{3\varepsilon}P_b \tag{4}$$

where S is mean strain tensor,$C_1, C_2, C_{1\varepsilon}$ are the constant.

The second considered model is *k*-ω model by Wilcox has the disadvantage of being highly sensitive to ω values specified in the freestream, see Menter [24]. For this reason, Menter [24] proposed the *k*-ω baseline (*BSL*) model, combining the *k*-ω model by Wilcox in the inner region of the boundary layer and the standard *k-ε* model in the outer wake and the free stream region. The equations for *k*-ω model are the following:

For turbulence kinetic energy:

$$\frac{Dk}{Dt}=\frac{\tau_{ij}}{\rho}\frac{\partial U_i}{\partial x_j}-\beta k\omega+\frac{\partial}{\partial x_j}\left[(\vartheta+\sigma_k\vartheta_t)\frac{\partial k}{\partial x_j}\right] \tag{5}$$

where ω is specific turbulent dissipation rate, τ_{ij} is turbulent stress tensor, ϑ_t is kinematic turbulent viscosity, and β, σ_k are the constant.

For specific dissipation rate:

$$\frac{D\omega}{Dt} = \alpha\frac{\omega}{k}\tau_{ij}\frac{\partial U_i}{\partial x_j} - \beta\omega^2 + \frac{\partial}{\partial x_j}\left[(\vartheta + \sigma_\omega\vartheta_t)\frac{\partial\omega}{\partial x_j}\right] \quad (6)$$

where α is the constant.

For turbulence kinetic energy in k-ω baseline (BSL) model:

$$\frac{Dk}{Dt} = P_k - \beta k\omega + \frac{\partial}{\partial x_j}\left[(\vartheta + \sigma_k\vartheta_t)\frac{\partial k}{\partial x_j}\right] \quad (7)$$

where $P_k = \min\left(\frac{\tau_{ij}}{\rho}\frac{\partial U_i}{\partial x_j}, 10\beta k\omega\right)$ is the generation of turbulence kinetic energy due to the mean velocity gradients.

Then for specific dissipation rate:

$$\frac{D\omega}{Dt} = \frac{\gamma}{\vartheta_t}P_k - \beta\omega^2 + \frac{\partial}{\partial x_j}\left[(\vartheta + \sigma_\omega\vartheta_t)\frac{\partial\omega}{\partial x_j}\right] + 2(1-F_1)\sigma_{\omega 2}\frac{1}{\omega}\frac{\partial k}{\partial x_i}\frac{\partial\omega}{\partial x_i} \quad (8)$$

where $\gamma, F_1, \sigma_\omega, \sigma_{\omega 2}$ are the constants.

In the case of the shear stress transport (SST) formulation is almost identical to the Menter BSL. Only one constant (σ_{k1}) and the expression for turbulent eddy viscosity are different:

$$\frac{D\omega}{Dt} = \alpha S^2 - \beta\omega^2 + \frac{\partial}{\partial x_j}\left[(\vartheta + \sigma_\omega\vartheta_t)\frac{\partial\omega}{\partial x_j}\right] + 2(1-F_1)\sigma_{\omega 2}\frac{1}{\omega}\frac{\partial k}{\partial x_i}\frac{\partial\omega}{\partial x_i} \quad (9)$$

For general calculation the double precision, the pressure-based fluent solver was used. As the phenomenon is stationary the steady-state model was selected. The first type of boundary condition was used for calculation. For the flow entering the domain the uniform velocity profile with turbulent intensively 5% and turbulent viscosity ratio equal to 10 were set up. The flow direction was set to normal to the inlet boundary. For the outlet boundary condition on the surface where the flow exits the domain, the static pressure was defined and the turbulence specification remained the same. The discretization schemes used in the calculation for both turbulent models were presented in Fig. 5.

When developing the numerical model of the orifice, several turbulence models were checked, but finally two were selected (k- ε and k-ω) as best reflecting the flow of fluid through the orifice. Calculations were made for different flow velocities. To reflect the actual flow profile, a suitably long inlet and outlet part of the pipeline was used. The lengths of the pipe were as follows: 60·D (diameters) i.e. 3 m before the orifice and 80·D i.e. 4 m behind the orifice. In the case of pressure take-off points, reference was made to standard 5167 [25], which describes the standard measuring orifices.

During the numerical tests, different points of stagnation pressure measurement by the differential pressure transmitter were analysed. For further analysis, two pressure measuring points D and $D/2$ were selected, which are located, respectively, 50 mm upstream of the orifice and 25 mm downstream of the orifice, in the cross-section along the axis of flow openings.

The prototype orifice has four openings; therefore, during the simulation, the influence of the location of pressure take-off points on the static backpressure values at these points in front of and behind the orifice was checked.

The solution controls that are under-relaxation factors remained unchanged, as the calculation ran smooth. For complex control of the process, the report definition for static pressure from all the stagnation pressure sampling points was created. During calculation, the equations residual were monitored for absolute criteria of 10^{-5}. The results of the calculations were considered complete when the pressure in the report definition fully stabilized and equations residual was under previously set criteria.

Figs. 6 and 7 present the results of the numerical analysis for turbulence models: *k-ε-realizable*, *k*-ω-*SST,* and *k*-ω-*BSL*. The simulations were carried out for four sizes of numerical grids (from 500,000 elements, which are denoted 500 k, to 9,000,000 elements, which are

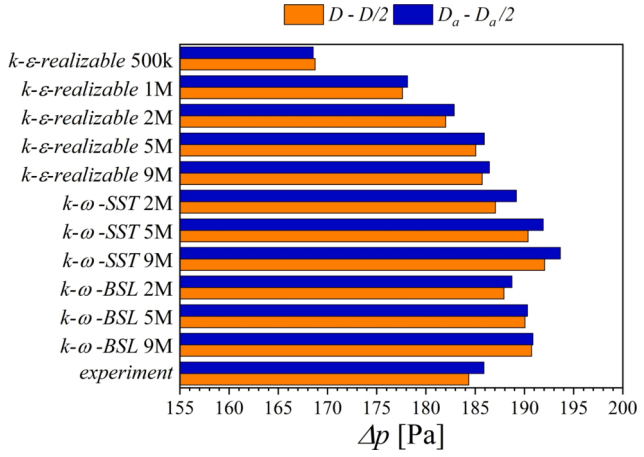

Fig. 6. Comparison of the values of the pressure difference at the pressure reception points *D-D/2* and D_a-$D_a/2$ for different numerical models and sizes of the computational grids against the experimental measurement: for fluid velocity 0.1 m/s.

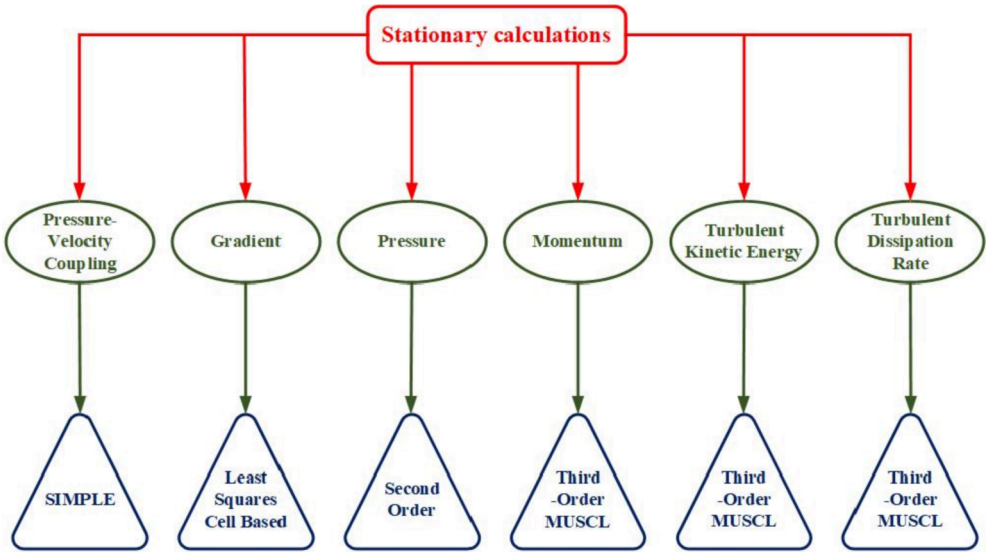

Fig. 5. Discretization schemes.

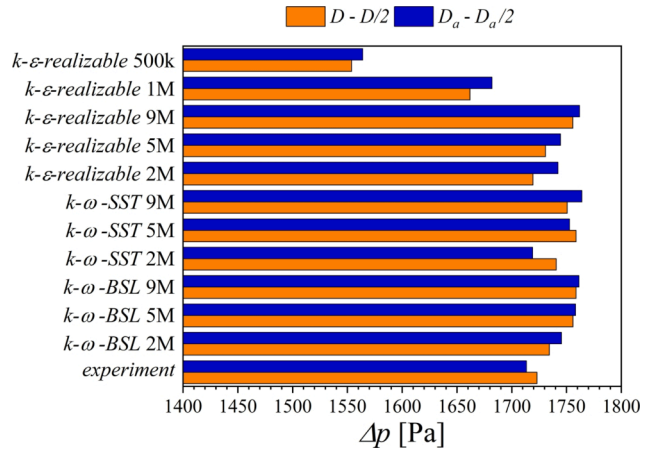

Fig. 7. Comparison of the values of the pressure difference at the pressure reception points *D-D/2* and D_a-D_a/2 for different simulation models and sizes of the computational grids, against the experimental measurement: for fluid velocity 0.3 m/s.

denoted 9M) and six different flow velocities of the medium: 0.1 m/s, 0.15 m/s, 0.2 m/s, 0.25 m/s, 0.3 m/s and 0.35 m/s. The article presents the results only for the two flow rates of 0.1 m/s and 0.3 m/s.

The following designations were adopted for the pressure measurement points: (*D–D/2*) - in the cross-section along the axis of the flow openings, (D_a–D_a/2) - in the cross-section along the axis shifted by 45°, that is, in the axis between the flow openings.

The presented analyses have shown that the mesh with 2,000,000 elements is sufficient, as the 4.5 times increase of mesh size results only in less than 2% change in pressure difference, while the time and computing power needed to obtain this result increases several times.

The results obtained confirm that the adopted assumption of a mesh consisting of 2M elements, in this case, is completely sufficient, and at the same time significantly shortens the calculation time compared to meshes consisting of 5M and 9M elements. All solutions converged (that is, residues below 10^{-5}).

Finally, for the selected mesh, two turbulence models were selected, based on the test analyses *k-ε-realizable 2M* and *k-ω-BSL 2M* which generate similar results. Simulations were carried out for Reynolds numbers *Re* = 5000 and *Re* = 15,000, and for the water at a temperature equal to 20°C in the tested DN50 pipeline.

For the analysed models, *k-ε-realizable 2M* and *k-ω-BSL 2M*, the velocity and static pressure distributions in the area of the tested orifice are presented in Figs. 8-10. Fig. 8 shows the static pressure distribution given by the *k-ε-realizable 2M* model at a flow velocity of 0.3 m/s.

Figs. 9 and 10 show the velocity distributions and streamlines in the pipeline x-z plane for *k-ε-realizable 2M* and *k-ω-BSL 2M* turbulence models and for fluid velocity equal to m/s

We can infer from Figs. 8 and 9 that the recirculation distance does not exceed 2·*D* and that the recirculation ends soon behind the orifice. In this case, the multi-hole orifice acts as a stream straightener in the pipeline; the streamlines become parallel to each other.

Fig. 11 shows the static pressure distribution at a distance × from the orifice in the simulated DN50 pipeline for the *k-ε-realizable 2M* turbulence model and fluid velocity *υ* = 0.3 m/s (*Re* = 15,000).

Fig. 11 reveals a slight increase in static pressure just before the inflow side of the orifice, while on the downstream side the negative pressure area is observed, which gradually changes to overpressure with increasing distance from the orifice.

4. Experimental research

During measurement in the orifice (Fig. 1), the backpressure was measured in a straight DN50 pipeline. The lengths of the straight sections were: 46·*D* (2.3 m) before the orifice and 36·*D* (1.8 m) behind the orifice. The view of the measurement section with the orifice housing and the APR-2000/ALW transducer is shown in Fig. 12.

The backpressure at the tested orifice was measured using the APR-2000/ALW differential pressure transducer at the standardized pressure sampling points *D-D/2*. This transducer has the programmed differential pressure measurement range set at 0–2.4 kPa at the measurement error equal to 0.15% of the measured value and the output current signal of 4–20 mA. At the same time, an electromagnetic flowmeter PROMAG 30AT15 with the measurement range of q_v = 0–1.0 dm^3/s and the output current signal of 0–20 mA was used as a reference flowmeter for the flow measurement. The maximum error limit of the indication of the electromagnetic flowmeter PROMAG 30AT15 is ±(0.2%· q_v + 0.05%·1) [dm^3/s]. The flow parameters (current signals from the standard flowmeter and the differential pressure converter) were acquired by the measuring system, which included PC-5000 multimeters and PC-Link Plus SANWA software. The sampling time of the current signal was Δ*t* = 4 s. The experimental measurement was carried out on the test stand described in detail in [10,18]. The absolute static pressure in the measuring system did not exceed 125 kPa. The upper limit results from this range because of the possibility of carrying out tests on a measuring stand. The temperature of flowing water was measured and, based on the tables, corrections related to the change of density and kinematic

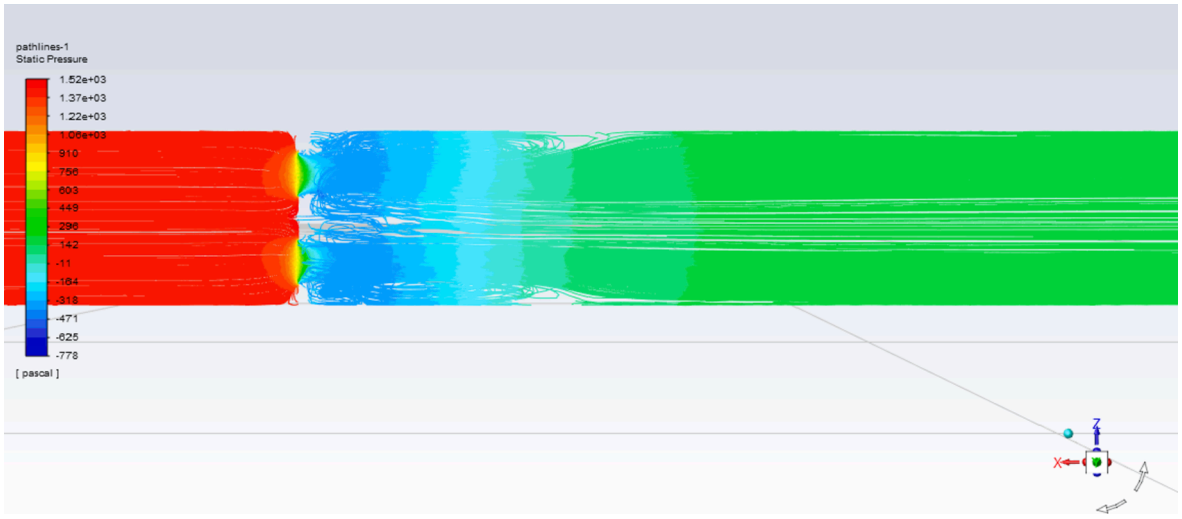

Fig. 8. Pressure distribution in the x-z plane: *k-ε-realizable 2M* model and fluid velocity 0.3 m/s.

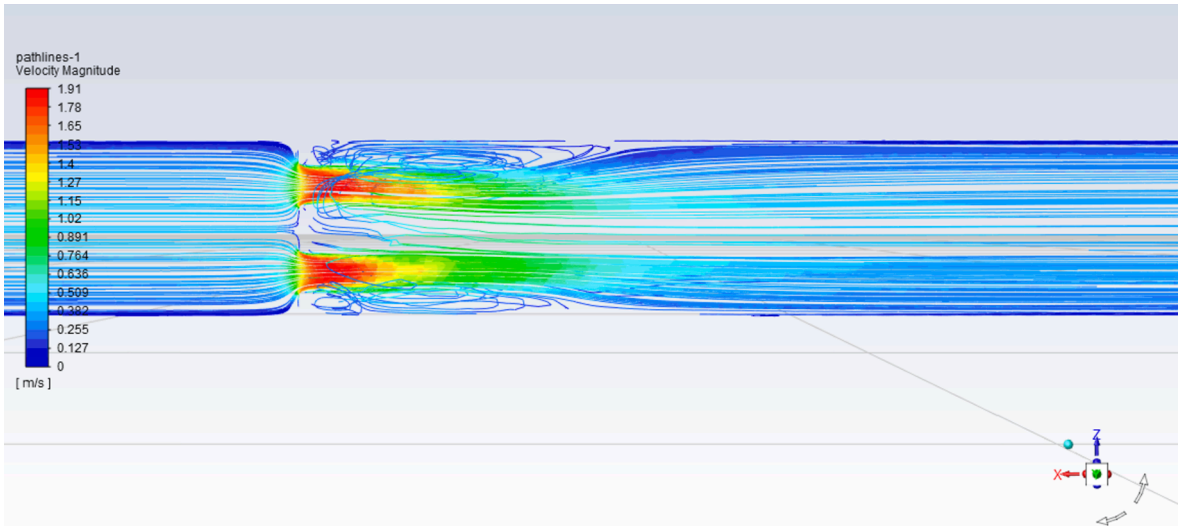

Fig. 9. Velocity distribution and streamlines in the pipeline x-z plane: *k-ε-realizable 2M* model and fluid velocity 0.3 m/s.

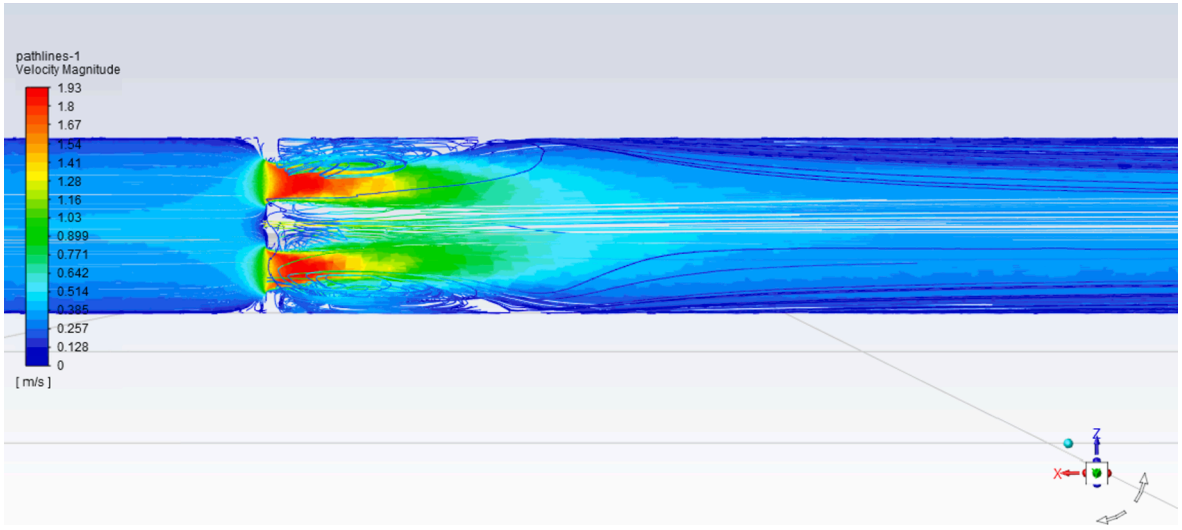

Fig. 10. Velocity distribution and streamlines in the pipeline x-z plane: *k-ω-BSL 2M* model and fluid velocity 0.3 m/s.

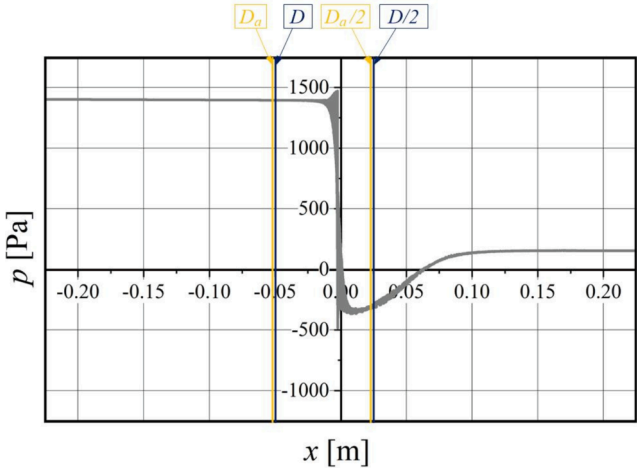

Fig. 11. Static pressure for the *k-ε-realizable 2M* turbulence model vs. distance × from the orifice plane ($x = 0$).

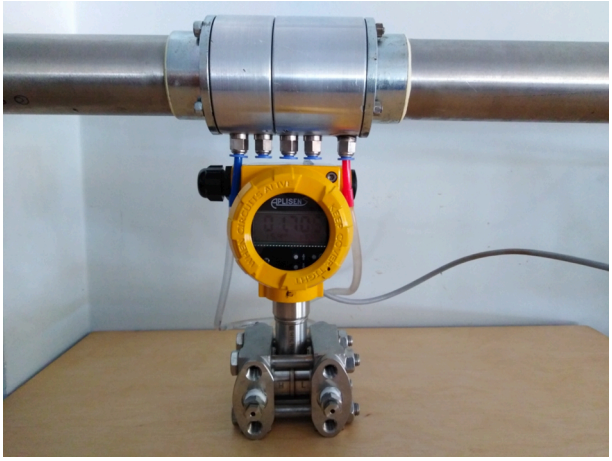

Fig. 12. View of the orifice housing with differential pressure transducer APR-2000/ALW.

viscosity of flowing water were included in the calculations.

The experimental measurements were carried out for 12 volumetric flow rates q_v ranging between 0.167 and 0.686 dm^3/s (which corresponded, respectively, to Reynolds numbers in the range of Re = 4,200–19,000). Measurements were made for a stabilized flow rate of the fluid at the points *D-D/2* (Table 1), and *Da-Da/2* (Table 2).

The last two columns of both tables present the value of the relative expanded uncertainty of measurement of the volume flow and the damming pressure at the orifice, respectively (determined with the dominant type B uncertainty, with the assumed uniform probability distribution of the instruments used and the coverage factor equal 2).

5. Results and discussion

Comprehensive metrological analysis of the studied orifice requires checking the compliance of selected mathematical models with the experimental values. For this purpose, calculations were performed, the results of which are presented in this chapter.

The values of the damming differential pressure obtained from the numerical analysis and experimental measurements at points *D-D/2* for the *k-ε-realizable 2M* and *k-ω-BSL 2M* turbulence models were compared. Fig. 13 presents the values of the average fluid flow velocities obtained from the numerical simulations with the *k-ε-realizable 2M* turbulence model against the experimental data.

Fig. 14 shows the comparison of the results of numerical simulation making use of the *k-ω BSL 2M* turbulence model with the experimental measurements.

To compare the convergence of the results obtained from numerical simulations and experimental measurements, the relative damming difference parameter (pressure difference upstream and downstream of the orifice) δ was determined as:

$$\delta = \frac{\Delta p_e - \Delta p_s}{\Delta p_e} \cdot 100\% \tag{10}$$

where: Δp_s and Δp_e are the pressure differences obtained from CFD simulation and experiment, respectively.

The values of the difference pressure Δp_e required for comparison in Eq. (10) corresponding to the constant water flow velocities v set in the numerical simulations were determined by approximating the results from Tables 1 and 2.

The results of the numerical calculations using the numerical model described in Section 3 and two selected turbulence models are presented in Tables 3 and 4.

Fig. 15 shows the δ distributions calculated according to formula (10) for the turbulence models *k-ε-realizable 2M* and *k-ω-BSL 2M*. The differences in δ values between the considered in this work models and the experimental measurements do not exceed 1.82% for *k-ε-realizable 2M* and − 1.54% for *k-ω-BSL 2M*.

The graphs in Figs. 13-15 and Tables 3 and 4 show that the selected models have interesting characteristics of convergence with the experimental data. In the range of low velocity, i.e. below 0.2 m/s, *k-ω-BSL 2M* model shows greater compliance with the experiment. For velocity above 0.2 m/s, *k-ε-realizable 2M* model, which in this range is more compatible than *k-ω-BSL 2M* model. To be able to better investigate the accuracy of mathematical modelling with experimental data, statistical analyses were performed.

To evaluate the phenomena occurring during the flow of liquid through the tested multi-hole orifice, the statistical analysis was per-

Table 2
Experimental measurements at points D_a-D_a/2.

T [°C]	q_v [dm^3/s]	Δp_e [Pa]	v [m/s]	$\nu \cdot 10^{-7}$ [m^2/s]	Re [−]	$U(q_v)$ [%]	$U(\Delta p_e)$ [%]
20.35	0.166	129.7	0.084	1.002	4,214	0.580	3.209
20.55	0.254	312.9	0.129	0.9967	6,487	0.459	1.330
20.85	0.347	592.4	0.177	0.9896	8,930	0.398	0.703
21.10	0.415	851.3	0.211	0.9837	10,740	0.371	0.489
21.45	0.459	1,043.3	0.234	0.9756	11,984	0.357	0.399
21.80	0.450	1,190.5	0.250	0.9676	12,899	0.349	0.350
21.40	0.525	1,368.9	0.267	0.9767	13,690	0.341	0.304
22.15	0.562	1,571.3	0.286	0.9596	14,924	0.334	0.265
22.25	0.595	1,761.9	0.303	0.9574	15,844	0.328	0.236
22.30	0.625	1,936.7	0.318	0.9563	16,642	0.324	0.215
22.30	0.657	2,143.5	0.335	0.9563	17,511	0.319	0.194
22.20	0.687	2344.3	0.350	0.9585	18,258	0.305	0.178

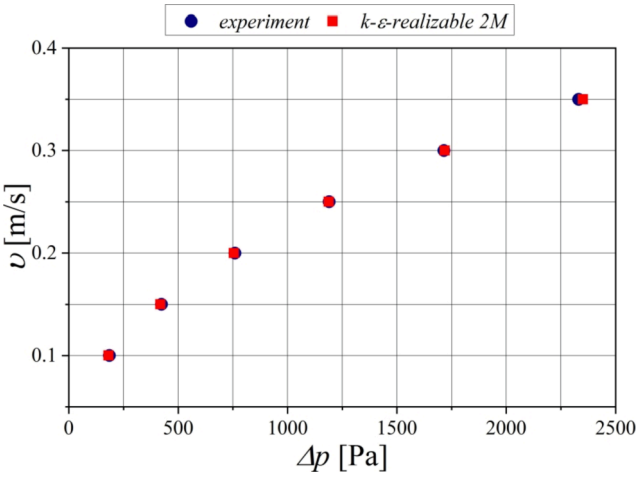

Fig. 13. Average fluid flow velocity as a function of the pressure difference obtained from numerical simulation with *k-ε-realizable 2M* turbulence model compared to the experimental measurements.

Table 1
Experimental measurements at points *D-D/2*.

T [°C]	q_v [dm^3/s]	Δp_e [Pa]	v [m/s]	$\nu \cdot 10^{-7}$ [m^2/s]	Re [−]	$U(q_v)$ [%]	$U(\Delta p_e)$ [%]
23.35	0.167	133.0	0.085	0.9332	4,552	0.578	3.129
23.45	0.255	316.2	0.130	0.9311	6,973	0.458	1.316
23.55	0.347	588.5	0.177	0.9289	9,499	0.398	0.707
23.65	0.417	856.7	0.212	0.9268	11,445	0.370	0.486
23.75	0.460	1,045.7	0.235	0.9247	12,680	0.357	0.398
23.85	0.488	1,176.0	0.249	0.9225	13,468	0.350	0.354
23.90	0.526	1,362.2	0.268	0.9215	14,523	0.341	0.306
23.90	0.593	1,556.3	0.285	0.9215	15,481	0.330	0.267
23.85	0.593	1,735.4	0.302	0.9225	16,362	0.329	0.240
23.75	0.624	1,925.2	0.318	0.9247	17,193	0.324	0.2162
23.20	0.656	2,126.8	0.334	0.9365	17,845	0.319	0.196
23.40	0.686	2,322.6	0.349	0.9321	18,738	0.316	0.179

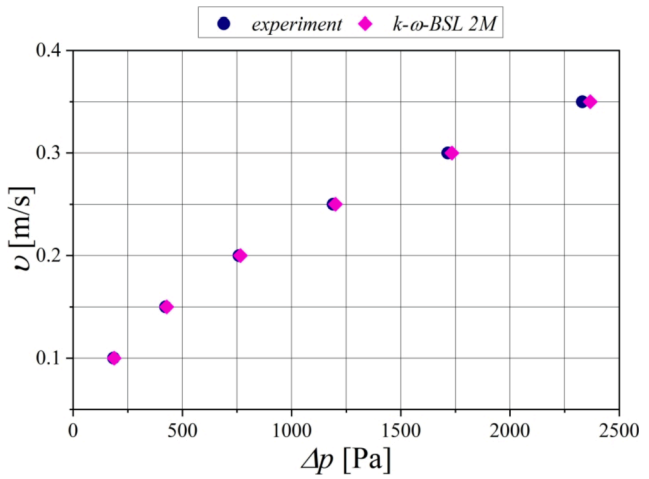

Fig. 14. Average fluid flow velocity as a function of the pressure difference obtained from numerical simulation with *k-ω-BSL 2M* turbulence model compared to the experimental measurements.

Table 3
Comparison of the numerical Δp_s and experimental Δp_e results for the turbulence model *k-ε-realizable 2M*.

υ [m/s]	Δp_e [Pa]	Δp_s [Pa]	δ [%]
0.10	185.4	182.0	1.82
0.15	423.6	418.9	1.11
0.20	759.3	754.6	0.61
0.25	1,190.4	1,188.6	0.15
0.30	1,715.0	1,719.5	−0.26
0.35	2,331.2	2,351.1	−0.85

Table 4
Comparison of numerical Δp_s and experimental Δp_e results for the turbulence model *k-ω-BSL 2M*.

υ [m/s]	Δp_e [Pa]	Δp_s [Pa]	δ [%]
0.10	185.4	187.9	−1.37
0.15	423.6	428.4	−1.12
0.20	759.3	765.6	−0.84
0.25	1,190.4	1,200.8	−0.87
0.30	1,715.0	1,734.2	−1.12
0.35	2,331.2	2,367.2	−1.54

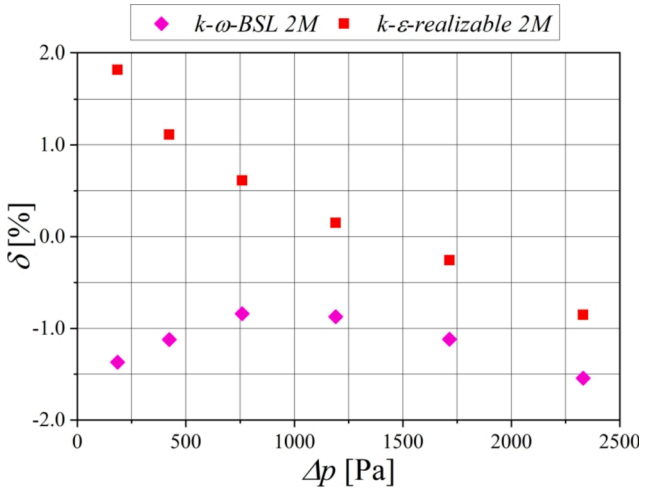

Fig. 15. Comparison for δ distributions the turbulence models *k-ε-realizable 2M* and *k-ω-BSL 2M*.

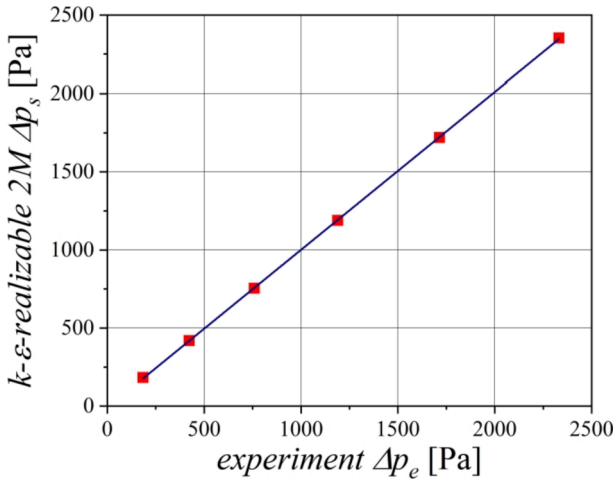

Fig. 16. Comparison of experimental data with numerical simulation data for the *k-ε-realizable 2M* model. Determination coefficient R^2 is equal to 0.99997.

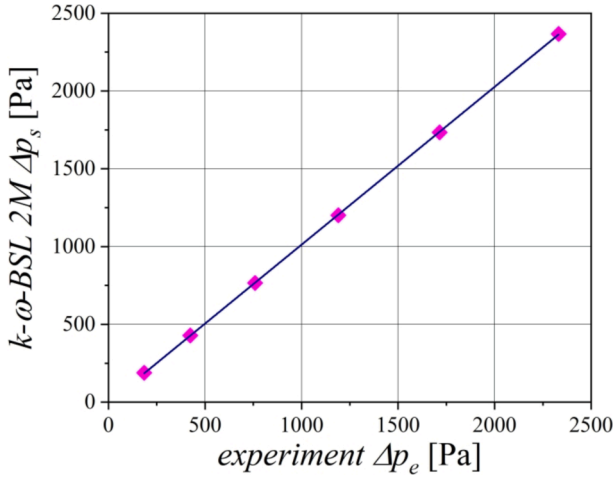

Fig. 17. Comparison of experimental data with numerical simulation data for the *k-ω-BSL 2M* model. Determination coefficient R^2 is equal to 0.99998.

formed based on cross-plot diagrams, as presented in Fig. 16 and Fig. 17. To estimate the similarity of the data sets obtained experimentally and from numerical simulations, a line given by the equation:

$$\Delta p_s = a \cdot \Delta p_e + b \tag{11}$$

where a is the slope and b is the intercept and was fitted using the least-squares method.

The equation describing the data presented in Fig. 16 is:

$$\Delta p_s = 1.0105 \cdot \Delta p_e - 10 \tag{12}$$

and in Fig. 17 is as follow:

$$\Delta p_s = 1.0149 \cdot \Delta p_e - 3.2 \tag{13}$$

Analysis of determination coefficients R^2 indicates that for both turbulence models, i.e. *k-ε-realizable 2M* and *k-ω-BSL 2M*, the similarity of the compared sets is close to 100% with a slight difference in favour of *k-ω-BSL 2M*. The correlation with the experimental data for *k-ε-realizable 2M* is 99.997%, while for *k-ω-BSL 2M* it is 99.998% which shows very high accuracy for proposed numerical models.

To assess the usefulness of the considered models, the obtained coefficients of the matching lines should also be additionally analysed. For the turbulence model *k-ε-realizable 2M*, the slope a is closer to the value

1.0 than for the turbulence model *k-ω-BSL 2M*. Such values of coefficients *a* and *b* have consequences in terms of the applicability of each of these models. These values indicate that the *k-ω-BSL 2M* model will perform better for lower differential pressure values (due to a higher value of coefficient *a* and a value of *b* close to zero). On the other hand, the *k-ε-realizable 2M* model will be more adequate in applications for large Δp values, as the higher value of coefficient *b* will not matter as much as the slope *a*.

The presented calculations and analyses show that the selection of the appropriate model is directly related to the velocity range for which one wants to perform the metrological analysis of the multi-orifice orifice. Hence, for $Re < 10{,}000$ a better model is *k-ω-BSL 2M*, while for $Re > 10{,}000$ the authors recommend using the *k-ε-realizable 2M* model.

6. Conclusion

The article presents the results of the simulation and experimental tests for a 4-hole orifice with module $m = 0.25$ installed in a pipeline with a flow diameter of DN50. The research study was carried out in the area of developing turbulent flow, that is, in the range of Reynolds numbers $Re = 4{,}200$–$19{,}000$.

The detailed numerical simulation was carried out with Ansys Fluent for two turbulence models: *k-ε-realizable* and *k-ω-BSL*. Static pressure and water velocity distributions in the pipeline were determined. It has been found that the *k-ω-BSL 2M* model better describes the flow for lower differential pressures. In turn, the *k-ε-realizable 2M* model shows better agreement with the experiment for large values of Δp.

The results obtained from numerical simulations indicate the possibility of using shortened straight sections before and after the orifice, with a length equal to two pipe diameters ($2 \cdot D$). Analysis of the simulation data shows that behind the orifice, a very short stream discontinuity area is formed, and then the flow stabilizes. As the fluid moves in the pipeline, the vortices that form in this area turn into parallel stabilized streams. This is an important advantage of a multi-hole orifice that can be utilized in industrial and technological systems. Industrial installations are often characterized by short straight sections resulting from the limited built-up area. In these sections, it is possible to install a multi-hole orifice-based measuring system that will ensure satisfactory accuracy of flow rate measurement in the flowing liquid.

The experimental tests were carried out for selected flow rates q_v ranging between 0.167–0.686 dm^3/s (which corresponded to Reynolds numbers in the range of $Re = 4{,}200$–$19{,}000$). Measurement back pressure on the tested orifice was measured at standard pressure points *D-D/2*. To compare the convergence of the results of the numerical simulation and the experiment, the relative pressure difference δ for the tested *k-ε-realizable 2M* and *k-ω-BSL 2M* turbulence models, related to the experimental data, was determined. It was found that the maximum difference between the analysed models is 3.36% and occurs for small values of Δp. The differences in δ values between the tested models and the experiment did not exceed 1.82% for *k-ε-realizable 2M* and −1.54% for *k-ω-BSL 2M*.

Based on the results obtained from numerical and experimental studies and previous publications by the authors [10], it was found that flow meters based on multi-hole orifices exhibit better metrological properties than flow meters based on a standard centric orifice. They are characterized by a stable value of the discharge coefficient (approximately 2% higher than the discharge coefficient for the centric orifice) for Reynolds numbers $Re > 10{,}000$ [20].

It seems that the centric orifices used in the industrial measurements can be replaced with multi-hole orifices, therefore, they require further research.

CRediT authorship contribution statement

Anna Golijanek-Jędrzejczyk: Conceptualization, Methodology, Formal analysis, Writing – original draft, Writing – review & editing, Supervision. **Andrzej Mrowiec:** Conceptualization, Methodology, Investigation, Resources, Writing – original draft, Writing – review & editing. **Sławosz Kleszcz:** Methodology, Software. **Robert Hanus:** Validation, Writing – review & editing, Supervision. **Marcin Zych:** Conceptualization, Visualization, Validation, Writing – review & editing. **Marek Jaszczur:** Conceptualization, Methodology, Software, Writing – original draft, Visualization, Writing – review & editing, Supervision.

Declaration of Competing Interest

The authors declare that they have no known competing financial interests or personal relationships that could have appeared to influence the work reported in this paper.

Acknowledgements

The present work was partially supported by the Minister of Education and Science of the Republic of Poland (Grant AGH No. 16.16.210.476, and 'Regional Initiative of Excellence' program for years 2019–2022, project number 027/RID/2018/19) and by the Department of Geophysics Faculty of Geology, Geophysics and Environment Protection AGH University of Science and Technology No. 16.16.140.315.

References

[1] M.A. Crabtree, Industrial Flow Measurement, University of Huddersfield, 2009.
[2] P.P. Kremlowski, Raschodimiery i scetciki kolicestva, vescestv, Politechnika Saint Petersburg (2002) in Russian.
[3] A. Gondek, Flow meters that bank up the flow, Politechnika Krakowska (2009) in Polish.
[4] M. Turkowski, Flow metrology, O.W. Politechniki Warszawskiej, Warszawa, 2018 in Polish.
[5] B. Tomaszewska-Wach, M.R. Rząsa, M. Majer, Measurement of two-phase gas-liquid flow using standard and slotted orifice, IAPGOS 9 (2019) 30–33, https://doi.org/10.35784/IAPGOS.47 (in Polish).
[6] M.A. Mehmood, M.A. Ibrahim, A. Ullah, M.H. Inayat, CFD study of pressure loss characteristics of multi-holed orifice plates using central composite design, Flow Measurement and Instrumentation 70 (2019) 101654, https://doi.org/10.1016/j.flowmeasinst.2019.101654.
[7] D.S. Dhumal, Y.R. More, U.S. Gawai, Design, fabrication & analysis of multi-hole orifice plate, Int. J. Eng. Technol. 6 (2017) 353–357, https://doi.org/10.17577/IJERTV6IS060161.
[8] S. Huang, T. Ma, D. Wang, Z. Lin, Study on discharge coefficient of perforated orifices as a new kind of flowmeter, Exp. Therm. Fluid Sci. 46 (2013) 74–83, https://doi.org/10.1016/j.expthermflusci.2012.11.022.
[9] M. Taiyi, W. Dong, Z. Bingdong, L. Zonghu, Experimental on metering characteristics of multi-hole orifice, Nuclear Power Engineering 31 (2) (2010) 126–130.
[10] U. Otgonbaatar, E. Baglietto, N. Todreas, Methodology for characterizing representativeness uncertainty in orifice plate mass flow rate measurements using CFD simulations, Nucl. Sci. Eng. 184 (3) (2016) 430–440, https://doi.org/10.13182/NSE16-9.
[11] P. Piechota, P. Synowiec, A. Andruszkiewicz, W. Wędrychowicz, Selection of the relevant turbulence model in a CFD simulation of a flow disturbed by hydraulic elbow — comparative analysis of the simulation with measurements results obtained by the ultrasonic flowmeter, J. Therm. Sci. 27 (5) (2018) 413–420, https://doi.org/10.1007/s11630-018-1034-z.
[12] A. Golijanek-Jędrzejczyk, A. Mrowiec, R. Hanus, M. Zych, D. Świsulski, Uncertainty of mass flow measurement using centric and eccentric orifice for Reynolds number in the range $10{,}000 \leq Re \leq 20{,}000$, Measurement 160 (2020), 107851, https://doi.org/10.1016/j.measurement.2020.107851.
[13] V.S. Bagade, P.M. Suryawanshi, S.M. Nalavade, A review of multi-hole orifice plate, Int. J. Res. Appl. Sci. Eng. Technol. 7 (2019) 3197–3208, https://doi.org/10.22214/ijraset.2019.4536.
[14] A.Tomaszewski, T. Przybylinski, M.Lackowski, Experimental and Numerical Analysis of Multi-Hole Orifice Flow Meter: Investigation of the Relationship between Pressure Drop and Mass Flow Rate. Sensors 20 (2020) 7281; doi:10.3390/s20247281.
[15] K.J. Mahendra Babu, C.J. Gangadhara Gowda, K. Ranjith, Numerical Study on Performance Characteristics of Multi-hole Oriface Plate. IOP Conf. Ser. Mater. Sci. Eng. (2018) 376, doi:10.1088/1757-899X/376/1/012032.
[16] M. Durdewic, M. Bukurov, S. Tasin, S. Bikic, Experimental research of single-hole and multi-hole orifice gas flow meters. Flow Meas. Instrum. 70 (2019) 101615, doi:10.1016/j.flowmeasinst.2019.101650.

[17] C.Z. Hao, X.M. Song, Z.N. Jia, Influence of the hole chamfer on the characteristics of a multi-hole orifice flowmeter, Fluid Dyn. Mater. Process. 15 (2019) 391–401, https://doi.org/10.32604/fdmp.2019.07771.
[18] V.K. Singh, T.J. Tharakan, Numerical simulations for multi-hole orifice flow meter, Flow Meas. Instrum. 45 (2015) 375–383, https://doi.org/10.1016/j.flowmeasinst.2015.08.004.
[19] M. Moosa, M.H. Hekmat, Numerical investigation of turbulence characteristics and upstream disturbance of flow through standard and multi-hole orifice flowmeters, Flow Meas. Instrum. 65 (2019) 203–218, https://doi.org/10.1016/j.flowmeasinst.2019.01.002.
[20] A. Mrowiec, Uncertainty assessment for determining the discharge coefficient C for a multi-opening orifice, Appl. Sci. 10 (2020) 8503, https://doi.org/10.3390/app10238503.
[21] G. Romanik, J. Rogula, The novel solution of ball valve witch replaceable orifice. Numerical and field tests, Open Eng. 9 (2019) 253–259, https://doi.org/10.1515/eng.2019.0034.
[22] H.K. Versteeg, W. Malalasekera, An introduction to Computational Fluid Dynamics: The Finite Volume Method. Pearson Education, 2007.
[23] L. Davidson, Fluid mechanics, turbulent flow and turbulence modelling; Division of Fluid Dynamics Departament of Applied Mechanics Chalmers, University of Technology, Goteborg, Sweden, 2014.
[24] F.R. Menter, Two-Equation Eddy-Viscosity Turbulence Models for Engineering Applications, AIAA Journal 32 (8) (1994) 1598–1605, https://doi.org/10.2514/3.12149.
[25] EN ISO 5167-1: 2003 Measurement of fluid flow by means of pressure differential devices inserted in circular cross-section conduits running full - Part 1: General principles and requirements.